COMPARISON OF THEORY, SIMULATION, AND EXPERIMENT FOR DYNAMICAL EXTINCTION OF RELATIVISTIC ELECTRON BEAMS DIFFRACTED THROUGH A SI CRYSTAL MEMBRANE*

L.E. Malin†, W.S. Graves, J.C.H. Spence, and C. Zhang, Arizona State University, Tempe, USA
R. Li, C. Limborg, E.A. Nanni, X. Shen, and S. Weathersby
SLAC National Accelerator Laboratory, Menlo Park, USA

Abstract

Diffraction in the transmission geometry through a single-crystal silicon slab is exploited to control the intensity of a relativistic electron beam. The choice of crystal thickness and incidence angle can extinguish or maximize the transmitted beam intensity via coherent multiple Bragg scattering; thus, the crystal acts as a dynamical beam stop through the Pendelösung effect, a well-known phenomenon in X-ray and electron diffraction. In an initial experiment, we have measured the ability of this method to transmit or extinguish the primary beam and diffract into a single Bragg peak. Using lithographic etching of patterns in the crystal we intend to use this method to nanopattern an electron beam for production of coherent x-rays. We compare the experimental results with simulations using the multislice method to model the diffraction pattern from a perfect silicon crystal of uniform thickness, considering multiple scattering, crystallographic orientation, temperature effects, and partial coherence from the momentum spread of the beam. The simulations are compared to data collected at the ASTA UED facility at SLAC for a 340 nm thick Si(100) wafer with a beam energy of 2.35 MeV.

INTRODUCTION

The electron beams produced by modern photoinjectors have sufficient quality (spread in energy and transverse momentum) to cleanly diffract through thin perfect crystal silicon membranes. By lithographically etching patterns in the Si, the diffraction can be spatially modulated at nanometer scale, producing nanometer spatial patterns in the electron beam. By laterally alternating strips of silicon of the correct thickness for dynamical extinction with very thin electron-transparent strips, we can spatially modulate the electron beam downstream of the crystal [1]. After acceleration to high energy these nanopatterned beams can be emittance-exchanged to produce bunching at nanometer scale in the time domain in preparation for lasing at x-ray wavelength in an undulator or inverse Compton scattering experiment [2].

As a first step to building this novel scheme, we are diffracting electrons through thin Si crystal membranes, varying the diffraction angle, and measuring the intensity of the primary beam and diffracted spots. We are developing a diffraction code for relativistic electrons using the multislice method and comparing its results both with the experiments and with the well-known electron microscopy software JEMS [3]. We will use the code to in the future to explore various crystal thicknesses and orientations to optimize the beam properties for nanopatterning.

MULTISLICE METHOD

The multislice method has long been established in the electron microscopy community as a method of calculating electron diffraction patterns in the dynamical regime [4], and has been successfully used to simulate experimental patterns for quite some time [5]. By dividing a crystal's potential into multiple layers along the electron's direction of travel and applying Schödinger's equation iteratively, the multislice method allows the electron wavefunction $\psi_n(x, y)$ to be calculated at exit from a crystal. Furthermore, it takes into account electrons experiencing multiple scattering events in a thick crystal - an aspect absent from kinematical theory. Equation (1) describes the wave function calculation at each layer n:

$$\psi_{n+1}(x, y) = p_n(x, y) * [t_n(x, y) \cdot \psi_n(x, y)] \quad (1)$$

where $p_n(x, y)$ is the Fresnel propagator, $t_n(x, y)$ is the transmission function, and $*$ is the 2-dimensional convolution. In the physical optics interpretation - the reasoning used in the method's creation [4] - the propagator accounts for near-field diffraction while the transmission function describes a phase grating.

To make the convolution calculation less computationally intensive, the Fast Fourier Transform and the convolution theorem are introduced to Eq. (1) [6]; given functions f and g integrable over the bounds of the convolution, we can write: $f * g = \mathcal{F}^{-1}[\mathcal{F}[f] \cdot \mathcal{F}[g]]$, where $\mathcal{F}$ and $\mathcal{F}^{-1}$ are the Fourier and inverse Fourier transforms respectively. After application we are left with

$$\psi_{n+1}(x, y) = \mathcal{F}^{-1}\{P_n(k_x, k_y) \cdot \mathcal{F}[t_n(x, y) \cdot \psi_n(x, y)]\} \quad (2)$$

where $P_n(k_x, k_y)$ is the Fourier transform of the real-space propagator. The precise forms of the transmission and propagator in the pertinent spaces with sample tilt (up to 1°) included are as follows:

$$P_n(k_x, k_y) = \exp[-i\pi\lambda\Delta z + 2\pi i\Delta z\alpha(k_x, k_y, \theta_x, \theta_y)] \quad (3)$$

where $\alpha(k_x, k_y, \theta_x, \theta_y) = k_x \tan\theta_x + k_y \tan\theta_y$, k_x and k_y are the x and y components of the wavenumber, θ_x and θ_x

* Work supported by NSF awards 1632780 and 1231306, DOE award DE-AC02-76SF00515, and the SLAC UED/UEM Initiative Program Development Fund.
† lemalin@asu.edu

Copyright © 2017 CC-BY-3.0 and by the respective authors

are the x and y components of the sample tilt, and Δz is the slice thickness;

$$t(x, y, \Delta z) = \exp[i\sigma V(x, y)\Delta z] \tag{4}$$

where σ is the relativistic electron interaction constant given by $\sigma = \frac{2\gamma m_0|e|\lambda}{4\pi\hbar^2}$, with m_0 the electron rest mass, γ the Lorentz factor, e the electron charge, λ the relativistic electron wavelength, and $\hbar$ the reduced Planck constant.

In Eq. (4), $V(x, y)$ is the crystal potential projected along the beam direction z that describes the potential within a distance Δz of the current layer; we approximate this by treating it as a sum of the individual atomic potentials of all the atoms in the layer. Additionally, the potential can be expressed as a sum of Fourier Coefficients, which are proportional to the the electron scattering factor and are weighted by a Debye-Waller temperature factor B according the expression $\exp[-Bs_{\vec{g}}]$, where $s_{\vec{g}} = \frac{sin\theta}{\lambda}$, θ is the Bragg angle of the $\vec{g}$ diffraction spot, and λ is the relativistic electron wavelength. The temperature factor causes increased attenuation of high-angle scattering with increasing temperature. As for determining values,there are numerous parametrizations that been calculated that allow the electron scattering factor [7] and the Debye-Waller factor [8] to be calculated for various elements and temperatures.

Partial Coherence

Partial coherence occurs when there is a spread in the momentum of the incident electron beam and is related to the concept of emittance. In the absence of a transverse magnetic field, we can write $p_x = m_0 c\beta\gamma x'$ where m_0 is the electron rest mass, c is the speed of light, β is the relativistic factor that appears in the Lorentz factor γ, and x' is the angle of the particle's trajectory. Since we can also write $\vec{p} = \hbar\vec{k}$, the normalized emittance of the beam can be expressed as follows:

$$\epsilon_n^x = \frac{\hbar}{m_0 c}\sqrt{\langle x^2\rangle\langle k_x^2\rangle - \langle xk_x\rangle^2} \tag{5}$$

where x is the particle position. A similar expression holds for the y-direction.

To match the momentum spread present in physical beams, we first consider an electron plane wave with wavefunction $\psi(\vec{x}, \vec{k_i}) = \exp[2\pi\vec{k_i} \cdot \vec{x}]$ where $\vec{k_i}$, is the deflection of the beam from the normal of the crystal as expressed in reciprocal space. To include this partial coherence, we sum over the angles and apply a weighting function $p(\vec{k_i})$, in this case the beam can be approximated with a Gaussian distribution. The resulting intensity is

$$I(\vec{x}) = \frac{1}{N}\sum_i p(\vec{k_i})|\psi_t(\vec{x}, \vec{k_i})|^2 \tag{6}$$

where $\psi_t(\vec{x}, \vec{k_i})$ is the transmitted wavefunction at exit from the crystal and N is the number of angles included in the sum. The components of k_i in Eq. (6) are the distributions used for the k_x and k_y of Eq. (5).

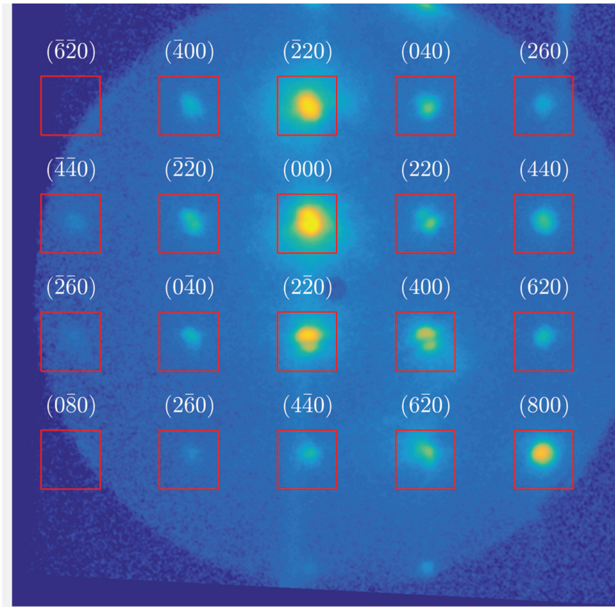

Figure 1: Measurements of Si(100) diffraction pattern on a scintillator for 2.35 MeV electrons (logarithmic scaling).

DIFFRACTION EXPERIMENT

A 340 nm thick Si(100) crystal was used to diffract a relativistic electron beam [9] at the ASTA Ultrafast Electron Diffraction (UED) facility at SLAC [10]. Of note is the method used to image the diffracted electrons: a P43 phosphor screen is positioned after the sample, perpendicular to the beam path; the light emitted by the scintillator is then reflected by a 45°in-vacuum mirror; and image from the phosphor screen is then focused by a large aperture coupling lens onto an Andor iXon Ultra 888 EMCCD. The sample holder itself can tilt along the x and y axes allowing for yaw and pitch scans; for this particular experiment, we fixed the yaw and varied along the pitch in so called pitch scans.

Data Processing

To interpret the images from the camera, we first subtracted the background caused by stray light hitting the CCD and then applied an averaging filter to remove hot pixels. To determine the intensity distribution, we summed over the counts within boxes encompassing each of the reflections (see Fig. 1 for the boundaries); the smaller box size was used to decrease the effect of light bleed from the phosphor screen to nearby pixels.

Examining select spots in Fig. 1, such as $(2\bar{2}0)$, (400), (220), and to some extent (000), Kikuchi lines are evident, the product of inelastic scattering during diffraction through the Si membrane. Due to the spatial variation this introduces in the background, inelastic effects could not be entirely removed during analysis. This deficit in the inelastic background causes the intensity of the affected reflection to be less than if the non-uniform background was removed.

Copyright © 2017 CC-BY-3.0 and by the respective authors

ISBN 978-3-95450-182-3

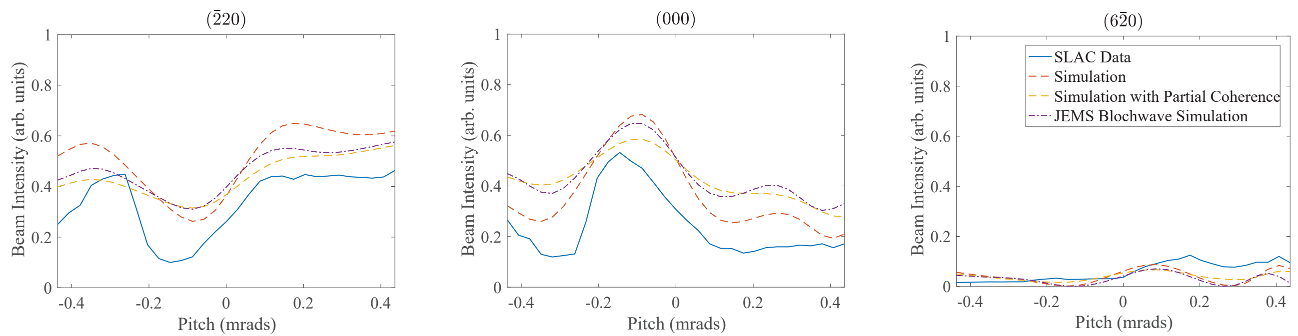

Figure 2: Comparison of measured and simulated intensity vs pitch angle for 3 different diffraction spots showing good qualitative agreement.

SIMULATION

To match the experimental beam, we simulated 2.35 MeV electrons with a Gaussian RMS width in reciprocal space k_s of 0.0192 Å^{-1}. As for the simulation parameters of the silicon, a single unit cell with a 128 x 128 pixel grid was used; when partial coherence was applied, an 8-by-8 unit cells was used to give the necessary resolution in reciprocal space and a 512 x 512 pixel grid for the proper resolution in real space. The maximum reciprocal lattice vector k_{max} used to calculate the potential in reciprocal space was 3.50 Å^{-1}. The membrane thickness was set to 340 nm. To more accurately model the intensities seen in the diffraction data, we normalized the particular spots we examined over only those spots that appeared in the experimental diffraction pattern without partial occlusion by the aperture present between the cathode and sample.

To determine the particular x and y angles associated with a particular pitch scan and thereby the propagator that must be used in the multislice calculation (see Eq. (3)), we first looked for diffraction patterns with a readily evident Laue circle. This circle is the intersection of the Ewald sphere with the observed plane of reflections, which passes through the origin of reciprocal space. Its center defines the in-plane wave-vector components k_x and k_y of the incident beam. From this, we could estimate the general area of the center of the Laue circle and perform mutislice calculations for tilts in the general vicinity. We then determined what orientation of yaw and pitch relative to our absolute tilts would minimize a qualitative least squares condition for the brighter spots in the pitch scan.

Comparison to Experiment

Using a least square minimization condition for the intensity simulation without partial coherence, we simulated a small range of sample rotations and found the intensity profiles of the two brightest reflections (000) and ($2\bar{2}0$) (after normalizing the two profiles to their respective maxima to allow just the relative variations to be compared) best matched a 33°clockwise rotation between the tilt apparatus and the camera with the center of the pitch scan occurring at a tilt of 7.7 mrad coinciding with the center of the Laue circle being located at $(4.9, 8.1, 0)$. The partial coherence case was then calculated along this path for comparison and the pitch scan was also simulated in JEMS using 87 Bloch-waves in the rocking curve function. The experimental data and the simulation outputs can be found in Fig. 2. The simulated values of the bright spots are greater than the experimental value, which is most likely due to insufficient removal of the inelastic background.

CONCLUSION

Using the multislice method, we simulated the experimental results obtained from the SLAC ASTA UED facility for a pitch scan at a fixed yaw, showing it can be a tool in determining both the sample thickness and orientation that will give a desired Bragg beam intensity, particularly for thin membranes where inelastic scattering is less prevalent. In future experiments, we will be able to determine beforehand the sample orientations and crystal thicknesses that will extinguish or maximize the Bragg beams; in combination with nanopatterned membrane and an emittance exchange, this will facilitate the production of the electron beam with nanoscale time domain variations necessary to lase at x-ray wavelengths.

ACKNOWLEDGEMENT

We thank Pierre Stadelmann for supplying a relativistic version of JEMS and for valuable discussion. We gratefully acknowledge financial support from NSF awards 1632780 and 1231306, the BioXFEL Science and Technology Center, U.S. DOE Contract No. DE-AC02-76SF00515, and the SLAC UED/UEM Initiative Program Development Fund. Travel support to IPAC'17 was provided by the NSF Division of Physics (Accelerator Science Program) and the Division of Beam Physics of the American Physical Society.

REFERENCES

[1] C. Zhang *et al.*, "Imaging the spatial modulation of a relativistic electron beam", in *Proc. 8th International Particle Accelerator Conference (IPAC'17)*, Copenhagen, Denmark, May 2017, paper MOPAB150.

Copyright © 2017 CC-BY-3.0 and by the respective authors

[2] E. A. Nanni, W. S. Graves, and D. E. Moncton, "Nano-modulated electron beams via electron diffraction and emittance exchange for coherent x-ray generation", arXiv:1506.07053, 2015.

[3] JEMS-SAAS, `http://www.jems-saas.ch/`.

[4] J. M. Cowley and A. F. Moodie, "The scattering of electrons by atoms and crystals. i. a new theoretical approach", *Acta Crystallographica*, vol. 10, no. 10, pp. 609–619, 1957.

[5] J. Zuo and J. Spence, *Advanced Transmission Electron Microscopy*. New York: Springer, 2017.

[6] K. Ishizuka and N. Uyeda, "A new theoretical and practical approach to the multislice method", *Acta Crystallographica Section A*, vol. 33, pp. 740–749, Sep 1977.

[7] E. J. Kirkland, *Advanced computing in electron microscopy*. New York: Springer, 2nd ed., 2010.

[8] V. Sears and S. Shelley, "Debye–waller factor for elemental crystals", *Acta Crystallographica Section A Foundations of Crystallography*, vol. 47, no. 4, pp. 441–446, 1991.

[9] E. A. Nanni *et al.*, "Measurements of transmitted electron beam extinction through si crystal membranes", in *Proc. 7th International Particle Accelerator Conference (IPAC'16)*, Busan, Korea, May 2016, paper TUPMY030, pp. 1611–1614.

[10] S. P. Weathersby *et al.*, "Mega-electron-volt ultrafast electron diffraction at slac national accelerator laboratory", *The Review of scientific instruments*, vol. 86, no. 7, p. 073702, 2015.

Copyright © 2017 CC-BY-3.0 and by the respective authors

ISBN 978-3-95450-182-3